VOLUME 8, NUMBER 2, FEBRUARY 2008

NANO LETTERS

On Total Internal Reflection Investigation of Nanoparticles by Integrated Micro-Fluidic System

Yanko E. Sarov,*[,†,‡] Ignac Capek,[§] Tzvetan B. Ivanov,[†] Katerina Zh. Ivanova,[†] Valentina A. Sarova,[||] and Ivo W. Rangelow[†]

MNES, IMNE, FEI, Technical University of Ilmenau, PF 100565, 98684 Ilmenau, Germany, Central Laboratory of Optical Storage and Processing of Information, Bulgarian Academy of Sciences, P.O. Box 95, 1113 Sofia, Bulgaria, Polymer Institute, Slovak Academy of Sciences, 9 Dubravska cesta, 842 36 Bratislava, Slovakia, and Institute of Electronics, Bulgarian Academy of Sciences, 72 Tsarigradsko Chaussee, 1784, Sofia, Bulgaria

Received December 13, 2007

ABSTRACT

We report on a novel sensor for characterization of nanoparticles colloidal suspensions. We employ a diffraction grating under total internal reflection for investigation of nanodisperse fluids passing through an integrated microfluidic channel. Dispersions containing polymeric, metallic, and ferromagnetic nanoparticles are studied. Using this device, we can accurately determine in real-time the specific refractive index for the nanoparticle suspension and the nanoparticle concentration. The nanoparticle concentrations can be calculated with a resolution of 0.3–0.5 wt % for polymeric nanoparticles, 0.03–0.05 wt % for metallic nanoparticles, and 0.05–0.1 wt % for ferromagnetic nanoparticles. This translates to an effective refractive index that can be determined with an accuracy of 7×10^{-4} for the polymeric and 2×10^{-4} for the metallic and ferromagnetic dispersions.

The intensive investigations on the field of micro total analysis systems (μ-TAS) motivate the further development of methods for microfluidic sensing. Here, a new technique that allows quick and accurate nanoparticle characterization is offered. A new device, an integrated diffraction grating and microfluidic channel, determines the optical properties and the concentration of fluid dispersed nanoparticles.

The optical scattering and extinction by small particles in liquids has been studied intensively.[1] However, the optical refraction of disperse systems has only been briefly mentioned,[2] although the value of the effective refractive index (ERI) is required to describe the light propagation through the material and its behavior at the medium interface. Critical angle refractometry takes advantage of the high sensitivity of the relative complex refractive index (RI) when optical reflectance occurs at an interface near the critical angle.[3] This

* Corresponding author. Phone: +49-3677-691590. Fax: +49-3677-693132. E-mail: ysarov@yahoo.com.
[†] MNES, IMNE, FEI, Technical University of Ilmenau.
[‡] Central Laboratory of Optical Storage and Processing of Information, Bulgarian Academy of Sciences.
[§] Slovak Academy of Sciences.
[||] Institute of Electronics, Bulgarian Academy of Sciences.

10.1021/nl073260o CCC: $40.75
Published on Web 12/29/2007

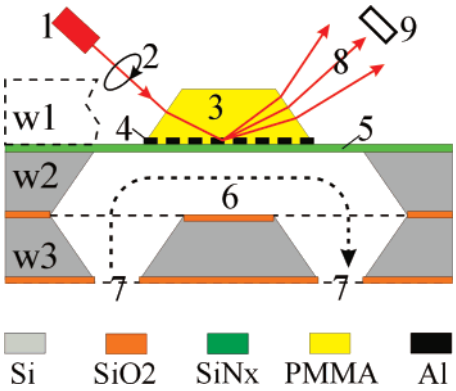

Figure 1. Structure of the microfluidic sensor and optical setup: (1) diode laser, (2) rotator of polarization, (3) PMMA microprism, (4) Al diffraction grating, (5) sealing layer, (6) microchannel, (7) in- and outlet nozzles, (8) diffraction pattern, and (9) photodetector.

makes it an ideal technique for measurements of the ERI of turbid and scattering media because extremely small optical changes, resulting from changes in the concentration, size, or composition of the particles can be detected.[2−8]

Complementary to total internal reflection (TIR) refractometry, different grating couplers on planar optical waveguides or fiber grating sensors use the evanescent field for (bio)chemical fluidic detection.[9−10] In such type of sensors, the diffraction grating (DG) has an indirect sensing function: to define the sensing area, where the waveguided propagation is frustrated and the evanescent field interacts with the liquid. Two techniques that directly exploit DGs for fluidic optical sensing are grating light reflection spectroscopy (GLRS)[11−14] and total internal reflection- diffraction grating (TIR-DG).[15−17] Both techniques are based on the transformation of a traveling wave to an evanescent one, which occurs when a transmitted diffracted wave disappears as it propagates through the DG material. The measured evanescent signal at the border between the grating and the underlying liquid media is very sensitive to the fluidic refractive n and absorption k indices. Additionally, the TIR-DG technique was found to be significantly more sensitive than the attenuated total reflection (ATR) technique due to interference enhancement.[15] A significant difference between TIR-DG and GLRS is that in GLRS the DG acts in amplitude transmission mode in the Raman−Nath regime. Thus, in the first method the matching condition for the disappearance of a transmitted order needs to be found by scanning the angle of incidence or the wavelength.[11−13] The behavior of a TIR-DG is quite different because the angle of incidence is always larger than the critical angle (the angle of TIR).[15−17] As a result, the light does not refract into the fluid; thus the TIR-DG always acts as a phase DG.[18] As such, TIR-DG offers advantages over GLRS because small variations in the fluidic RI are detected in real-time by changes in the diffracted light intensity without the need of any moving parts or spectral light analysis. GLRS has been already applied for liquids containing nanoparticles.[13−14] In our previous works, the first autonomous microrealization of a TIR-DG for uniform microfluid analysis is described.[19−20] Here, a TIR-DG is utilized for quantitative characterization of nanoparticle suspensions for the first time. A wide variety of liquid dispersions with polymeric, metallic, and ferromagnetic nanoparticles are investigated.

The principle of operation of the integrated TIR-DG microfluidic sensor can be illustrated with the help of Figure 1. The main element is a DG (4) situated between a transparent prism (3) and the investigated fluid (6). The light beam (1) is directed to the front refracting facet of the prism in such a way that the angle of incidence φ according to the prism base exceeds the critical angle for TIR φ_0.[15−17] The grating defines a periodic variation of the reflection: the mirrorlike reflection from the metal lines and TIR due to the line periodicity. The amplitude r_t and the phase Φ_t of the totally reflected light changes with variation of the fluidic optical constants.[15−16] The earlier studies show that small variations of the RI cause linear changes of Φ_t

$$\Delta\Phi_t^{\,s} = -\frac{2n\cos\varphi}{(1-n^2)\sqrt{\sin^2\varphi - n^2}}\Delta n,$$

$$\Delta\Phi_t^{\,p} = \Delta\Phi_s\frac{2\sin^2\varphi - n^2}{\sin^2\varphi(1+n^2) - n^2} \quad (1)$$

where n is the relative RI.

The case of weak fluidic absorption is accompanied by energy losses that only affect the TIR reflection amplitude r_t

$$r_t^{\,s,p} = 1 - \frac{\alpha d^{s,p}}{2} \quad (2)$$

where α denotes the fluidic absorption coefficient and $d^{s,p}$ is the penetration depth of the evanescent field. The superscripts s and p are related to s and p polarization, respectively.

The changes of the TIR light are connected to the interaction of the penetrating evanescent field with the induced dipoles of the fluidic molecules. However, the parameters of the light, reflected from the metal lines, remain constant. As a result of the interference between these two types of reflected light, a diffraction pattern (8) is created. The diffraction efficiency (DE) of the zeroth order for a grating with 50% duty factor is given by[19]

$$\eta^0 = (r_t^{\,2} + r_m^{\,2} + 2r_t r_m\cos(\Phi_t + \Phi_d - \Phi_m))/4 \quad (3)$$

where r_m and Φ_m are the amplitude and the phase of the reflected light from the metal lines and Φ_d is an additional phase shift due to the presence of a layer (5) which seals the grating.[20] Therefore, the substitution of eqs 1−2 in 3 proves the DE dependence on the fluidic optical constants.

The basic principles of the integrated sensor microfabrication are reported in our previous publications.[19−20] However, because nanoparticle dispersion analysis requires design modifications and improvements, a short summary of the microfabrication process is given here. The sensor is created by fitting together three Si <100> wafers, w1, w2, and w3

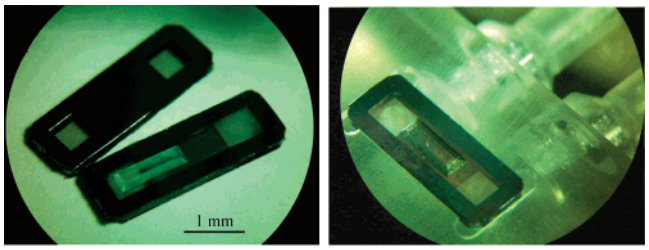

Figure 2. Pictures of the fabricated integrated microfluidic sensing systems: (a) single chips (one is turned back) and (b) a chip in its fluid-supply holder.

(Figure 1). In w1, the cavities, corresponding to the inverted prisms (3), are microfabricated by an anisotropic KOH etching. On the top of w2, a zero-stress SiN_x layer (5) is deposited. Subsequently, an Al DG (4) is realized by a lift-off technique. The SiO_2 on the bottom of w2 is patterned to create a mask for the microfluidic channel that will be etched later. The wafer w1 acts as an imprint mold to create the polymethylmethacrylate (PMMA) prism. The grating side of w2 is pressed onto w1, which is filled with liquid PMMA. Subsequently, the bonded wafers are etched in KOH until the SiN_x membrane is exposed. Thus, the microchannel (6) and the PMMA prism (3) are simultaneously realized. The in- and outlet nozzles (7) are etched by potassium hydroxide (KOH) in w3. Finally, w3 is bonded to w2 sealing the microchannel.

There are several major differences in respect to the previously produced sensors. First, by reducing the channel's surface dimensions three times and by using thinner w2 and w3 wafers, we reduce the sensor's flow volume an order of magnitude. In addition, we replace Cr with Al as the DG material so that the reflection amplitude from the metal lines approaches 100% for both polarizations and thus higher diffraction efficiency for all orders is achieved. Finally, we shrink the grating period from 10 to 2 μm to achieve higher angular divergence of the diffraction orders and permit closer spatial situation of the photodetector(s). Pictures of the fabricated microfluidic sensor are shown Figure 2.

Different types of nanoscale dispersions with polymeric, metal, and ferromagnetic particles have been investigated. The polymeric dispersions have poly(2-ethylhexyl acrylate) (PEHA), poly(methyl metacrylate) (PMMA) and poly(vinyl acetate) (PVAc) particles sized at 54, 49, and 68 nm, respectively and were prepared by (mini)emulsion polymerization. Nonionic emulsifier polyoxyethylene sorbitan monolaurate (Tween 20) is used as a stabilizer. The metal dispersions contain sub 10 nm Ag, Fe, or Co nanoparticles realized by stirring aqueous solutions of the corresponding metal salt ($AgNO_3$, $FeCl_2$, or $Co(CH_3COO)_2$) in the presence of a novel carboxymethyl starch as a stabilizer (an inverse microemulsion technique). The ferromagnetic dispersions contain sub 5 nm Fe_3O_4 and $CoFe_2O_4$ nanoparticles prepared by high-temperature precipitation from their respective reaction mixtures, which contained either $Fe(acac)_3$ or $Co(acac)_3$ salts, a high-boiling solvent, a stabilizer (oleic acid), and reducing agents (di-alkylols). After precipitation, the ferromagnetic particles were redispersed in hexane.

The dependence of the ERI, n, on the concentration, c, and the value of their specific RI Increment (SRII), dn/dc, of all dispersions used here have been reported in a recent work.[21] These measurements are made with an automatic refractometer implementing the method of the disappearing diffraction pattern.[21−22] It is a modified critical-angle method, which is feasible for dense scattering and turbid media.[22] The precision of the refractometric data is 2×10^{-4}. The effective absorption index (EAI) of the dispersions is measured by a light transmission from a 5 μm thick cell.

The operation setup is illustrated in Figure 1. The light of a red diode laser (1) with $\lambda = 633$ nm is directed to the front prism facet at an angle of incidence, which exceeds the critical angle by an angular deviation, $\delta = \varphi - \varphi_0$. The value of δ for each type of dispersion is critical and is theoretically calculated under conditions that simulate the diffraction behavior of the integrated sensor. Two requirements must be met: (i) the TIR condition must be fulfilled for the whole range of the expected RI and (ii) the TIR phase change due to the optical constant variation must be small to ensure linear detection. The smallest value of δ that meets these conditions is chosen (the smaller δ results in higher sensitivity[15−17]). On the basis of these requirements, δ is set to $\delta = 1.0°$ for the metal, $\delta = 1.2°$ for the ferromagnetic, and $\delta = 2.5°$ for the polymeric dispersions. The polarization direction is set at the rotator of polarization (2). For several important reasons, the photodetector (9) measures the DE η of the zeroth order of the pattern (8). First, the zeroth diffraction order is of the strongest orders. Moreover, the gradient of η is about 2 times higher compared to that of the $\pm$first diffraction orders, because the -1 and $+1$ orders are simultaneously exchanging energy with the zeroth order.[21] Thus, measurements of η have smaller relative error. In addition, the parasitic signal from the geometrical reflection and low-angle scattering can be easily extracted by measuring the output of the photodetector in a differential regime. Moreover, the behavior of all high-order diffracted waves is opposite to that of the zeroth (as a consequence of the constant total diffracted power).[20] Finally, using only one photodetector simplifies the experiments and the processing of the data.

The integrated sensor response is defined and measured as the relative DE change $\delta\eta = (\eta - \eta_0)/\eta_0$, where η is the zeroth order DE for a given dispersion and η_0 corresponds to the DE for the carrier liquid. The sensitivity of the integrated detector to the microfluidic RI variation is calibrated using aqueous solutions of sucrose, which have a linear dependence of their RI, n, on concentration c: $\Delta n = 1.45 \times 10^{-3} c$.[22] The calibration is made at the critical angles and δ's relevant for each type of nanoparticle dispersions studied. The calibration results for the response $\delta\eta$, plotted versus the RI increment $\Delta n = n - n_0$ are shown in Figure 3. The measurements with water ($n_0 = 1.332$) as the carrier liquid and angular deviation of $\delta = 1.0°$ and $\delta = 2.5°$ are

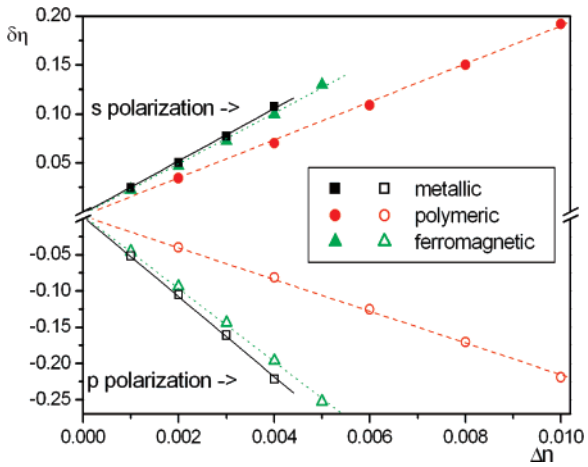

Figure 3. Relative variation of the DE with the RI of sucrose aqueous solutions.

Table 1. A Gradient of the Relative DE Change $\delta\eta$ with the Fluidic RI $s_r = d(\delta\eta)/d(\Delta n)$

		metal $n_0 = 1.332$, $\delta = 1.0°$	polymer $n_0 = 1.332$, $\delta = 2.5°$	ferromagnetic $n_0 = 1.374$, $\delta = 1.2°$
$s_r = d(\delta\eta)/d(\Delta n)$	s	26.81	19.42	25.94
	p	−55.80	−21.88	−50.42

presented by squares and triangles, respectively. The experiments with hexane-based dispersions ($n_0 = 1.374$) and $\delta = 1.2°$ are simulated by using sucrose solutions with a concentration of $c = 29.1$ wt %, and RI $n = 1.374$ as the reference carrier liquid. The corresponding results are represented by circles. In these and in all the following experiments, the filled signs correspond to s polarization of the light, while the hollow signs correspond to the orthogonal p polarization. The $\delta\eta$ gradient with RI, $s_r = d(\delta\eta)/d(\Delta n)$ for the three cases is determined by a linear fit of the calibration data and is presented in Table 1.

Figure 4 shows the results obtained by the integrated sensor for aqueous dispersions with polymeric nanoparticles. Figure 5 presents the investigation of aqueous dispersions with metallic nanoparticles, while Figure 6 deals with ferromagnetic nanoparticles, dispersed in hexane. In all of these experiments, the relative DE response $\delta\eta$ is plotted versus the concentration of the particles, expressed in wt %. The results from Figures 4, 5, and 6 possess several resemblances. First, for all studied dispersions the relative DE change is positive at s polarization (the zeroth order gains energy at an increase of the concentration and, respectively, of the ERI). The opposite response occurs for the p polarization; the η_0 diminishes for higher c. Such peculiarity of the polarization behavior is typical for a phase performance of the TIR-DR, that is, when transparent fluids are sensed[20] (no absorption or $r_t = 1$). The energy redistribution of the diffraction pattern in this regime is determined by the variations of the TIR phase Φ_t, caused by RI changes. Theoretical explanation about the effect of the polarization is the difference of the TIR phase for s and p polarization, which is close to π.[23] Hence, when the RI is changed and

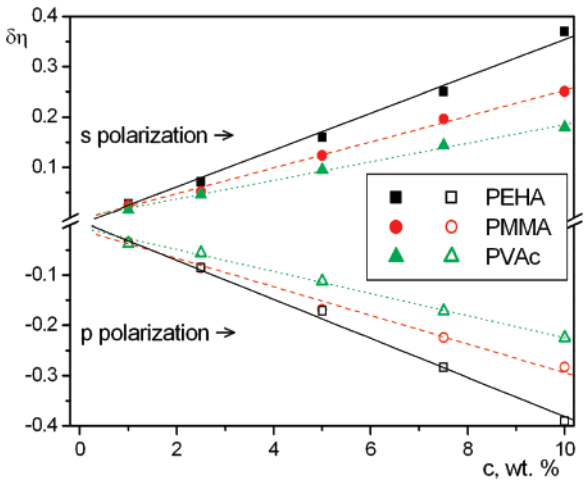

Figure 4. Relative variation of the DE with the concentration and the type of polymeric nanoparticles in water ($n_0 = 1.332$, $\delta = 2.5°$).

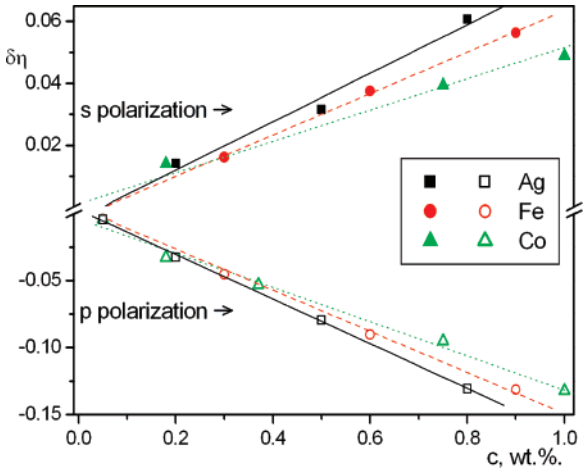

Figure 5. Relative variation of the DE with the concentration and the type of metallic nanoparticles in water ($n_0 = 1.332$, $\delta = 1.0°$).

the contribution of the cos term to the DE η (eq 3) is positive for one of the polarizations, the related contribution for the orthogonal polarization is negative.

The second similarity is the linear response of the integrated sensor. It is proven by the comparison of the experimental data from Figures 4, 5, and 6 with the linear fits (the lines in the figures). The maximum discrepancy between them is below the experimental error of 5% for all studied dispersions. Besides, the sensor response is always stronger for the dispersions with higher SRII, as reported in ref 21. This fact supports the suggestion that $\delta\eta$ is mainly caused by the TIR phase changes due to the variation of the fluidic RI.

The reported results for the concentration response for all three types of dispersions can be further used in two ways. First is the concentration analysis. The $\delta\eta$ gradient with the concentration of the nanoparticles s_c is determined as the slope $s_c = (d(\delta\eta))/dc$ of the linear fits from the data from Figures 4, 5, and 6. The resolution to the concentration of the nanoparticles Δc, corresponding to experimental uncertainty of the concentration response $\Delta(\eta)$ is given by: Δc

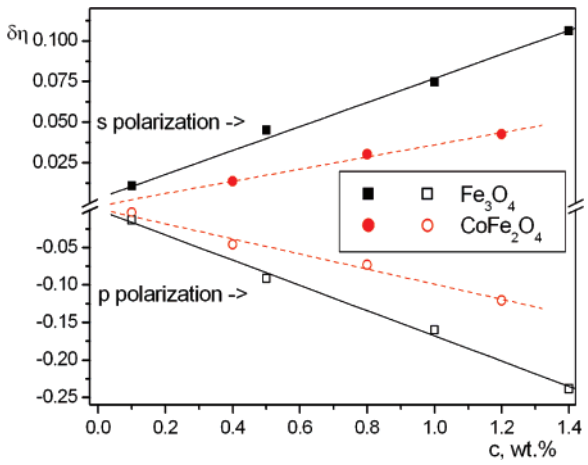

Figure 6. Relative variation of the DE with the concentration and the type of ferromagnetic nanoparticles in hexane ($n_0 = 1.374$, $\delta = 1.2°$).

$= |\mathrm{d}(\delta\eta)/\mathrm{d}c|^{-1}\,\Delta(\delta\eta) = |s_c|^{-1}\,\Delta(\delta\eta)$. The average experimental error is determined to be 5% as a statistical quadratic deviation of the measured data from the linear fits. Table 2 presents the values of s_c and Δc, determined for each type of dispersion.

The second application is the determination of the ERI and the SRII. This can be achieved in conjunction with calibration results. The effective SRII N_{SRII} of a given medium is defined as $N_{SRII} = \mathrm{d}n/\mathrm{d}c = (\mathrm{d}(\delta\eta)/\mathrm{d}c)(\mathrm{d}(\delta\eta)/\mathrm{d}(\Delta n))^{-1} = s_c/s_r$. The value of N_{SRII} can be determined in two independent ways using the experiments at s and p polarization. The corresponding results, as well the average value $\bar{N}_{SRII} = (N_{SRII}^{p} + N_{SRII}^{s})/2$ are presented in Table 2 and compared to the reference values.[21] The RI resolution, which corresponds to the calculated effective RI, is given by $\Delta n = |\mathrm{d}(\delta\eta^{calibr})/\mathrm{d}(\Delta n)|^{-1}\,\Delta(\delta\eta^{n-part}) = |s_r|^{-1}\Delta(\delta\eta^{n-part})$, where the derivative $\mathrm{d}(\delta\eta^{calibr})/\mathrm{d}(\Delta n)$ is found from the calibration experiment and the experimental uncertainty $\Delta(\delta\eta^{n-part})$ from the investigation of the dispersion with nanoparticles. These results are also presented in Table 2. The obtained concentration resolution is 0.3 ÷ 0.5 wt % for the polymeric, 0.03 ÷ 0.05 wt % for the metallic, and 0.05 ÷ 0.1 wt % for the ferromagnetic nanoparticles. The effective refractive index can be calculated with an accuracy of 7×10^{-4} for polymeric and 2×10^{-4}- for metallic and ferromagnetic dispersions.

Let us discuss the calculated values for the SRII, obtained at s and p polarization and their difference with the reference values. As can be seen from Table 2, the experimental SRII for both polarizations in fact coincide for the polymeric dispersions. In contrast, the sensor systematically detects lower SRII at s and higher SRII at p polarization for the absorbing dispersions. This deviation is less than 5−10% for all metallic and ferromagnetic dispersions, which gives in RI error below $1.10^{-4} \div 2.10^{-4}$. Although for some applications such an error could be acceptable, it can be also seen that the average value $\bar{N}_{SRRI}$ in all cases coincides much better (2−4%) with the references. The earlier investigations of the TIR-DG sensors[15,17,20] have dealt either with pure transparent (variable n, $k = 0$) samples either with pure absorbing fluid (n = const, variable k). The first case is accompanied by an exchange of energy between the zeroth and the ±first diffraction orders (the strengthening of the zeroth order is connected with weakening of the ±first orders and vice versa). In addition, the zeroth order response to RI changes is opposite for the case of s and p polarization, as observed and discussed above. In contrast, the sensing of strongly absorbing fluids shows that the DE η decreases with the fluidic absorption[19−20] for all diffraction orders and for any polarization direction.[16,17,20] The case considered in this paper samples combines these two cases; both the ERI and the EAI of the nanodispersions depend linearly on their concentration. Experimentally, the EAI, related to a unit wt % concentration is of the order of 10^{-5} for the dispersion with polymeric and 10^{-4} for the metallic and ferromagnetic particles. Because the SRII is in the order of 10^{-3}, all the studied dispersions are weakly absorbing. Nevertheless, the nonzero EAI of the dispersions results in a decrease of the DE concentration response, which means a smaller absolute value of the derivative $s_c = (\mathrm{d}(\delta\eta))/\mathrm{d}c$ for s and a higher absolute value for p polarization. As a consequence, the influence of the EAI on the averaged SRII $\bar{N}_{SRRI}$, as defined and calculated above, is lowered. In addition, the difference

Table 2. Sensitivity and Resolution of Concentration and RI for the Different Studied Dispersions

		polymeric			metallic			ferromagnetic	
		PEHA	PMMA	PVAc	Ag	Fe	Co	Fe_3O_4	$FeCo_2O_4$
$s_c \times 10^2$	s	3.64	2.57	1.90	7.64	6.68	5.06	7.40	3.75
	p	−3.88	−2.84	−2.19	−16.64	−15.15	−12.58	−16.82	−10.05
Δc wt %	s	0.27	0.39	0.53	0.033	0.037	0.049	0.054	0.137
	p	0.26	0.35	0.46	0.030	0.033	0.040	0.051	0.089
$N_{SRRI}^{exp} \times 10^3$ (Figures 3−6)	s	1.85	1.32	0.98	2.85	2.49	1.89	2.85	1.45
	p	1.78	1.30	1.00	2.99	2.71	2.25	3.33	1.99
$\bar{N}_{SRRI} \times 10^3$		1.83	1.31	0.99	2.97	2.60	2.07	3.09	1.72
$N_{SRRI} \times 10^{3a}$		1.79	1.26	1.01	2.90	2.62	2.15	3.11	1.78
$\Delta n \times 10^4$	s	8	8	8	2	2	2	2	2
	p	7	7	7	2	2	2	3	3

[a] Ref 22.

between the concentration and the ERI, determined at the orthogonal polarization can be used to estimate the fluidic effective absorption simultaneously to determine the ERI. A rigorous theoretical demonstration is a subject of further investigations.

However, it is worthy to point out here that: (1) measurements with one polarization are correct for sensing of nanodispersions with negligible effective absorption; (2) measurements with two orthogonal polarizations can be used to increase the sensing accuracy and to estimate the absorption in the case of slightly absorbing nanofluids. Practically, the measurements with two polarizations can be easily run simultaneously and in real-time by setting the laser polarization at 45° and using one polarization beam-splitter to divide the two polarization components of the zeroth order light and two photodiodes to detect them.

The sensitivity of the microdevice can be further increased setting the angle of incidence closer to the critical angle, which means a smaller value of δ. The price of the higher accuracy is a shrunk measurement range,[19−20] because the proper operation requires the TIR condition to be fulfilled for all expected RI values. The limits of the accuracy depend on the possibility to keep stable the optical parameters of the continuous phase: temperature, salts content, purity, etc. Because the temperature gradient of the RI of water is below 1×10^{-4} K^{-1}, typical variations of the room temperature (± 1 °C) are acceptable for RI sensing with relative error of $\Delta n/n \sim 10^{-4}$. When a sensing with an order of magnitude higher accuracy is required, the fluidic temperature has to be controlled with a precision of ± 0.1 °C.

Apart from an optical and concentration analysis, the microfluidic system can be important for size determination only in limited cases. The requirement is the size of the particle to be comparable with the light wavelength.[4,8] Even then, the TIR refractometry shows a poor sensitivity, compared to the common particles size characterization techniques like transmission electron microscopy (TEM), atomic force microscopy (AFM), or dynamic light scattering (DLS). Nevertheless, the presented microfluidic sensor overcomes some of the disadvantages typical for these methods. For instance, TEM and AFM require drying of the samples, which can lead to coagulation or oxidation of the particles. Dilution of the samples is needed by DLS. In addition, DLS determines the hydrodynamical particle size, which can differ significantly from the size of the core particle (e.g., surface-functionalized particles). However, the main advantage of the TIR-DG system is its ability in real-time to monitor highly absorbing or scattering fluids without any pretreatment. Then, a comparison between TIR sensing, DLS and TEM would be worthy.

The TIR-DG system can also be used to determine additional characteristics of the nanoparticle dispersion. For instance, by comparing the value of the SRII, unknown nanoparticle dispersions can be identified. In addition, the calculated concentration can be used to estimate the degree of polymerization during the preparation of a sample, an amount of residual precursor and an amount of unpolymerized monomer in real-time. Furthermore, the TIR device can be used to detect coagulation or precipitation of particles in dispersion.

The reported results clearly show that the TIR-DG system can be used to analyze nanoparticle dispersions, detecting the change of the diffraction efficiency as a function of concentration and the ERI. Because we use established fabrication techniques and batch-processing, we can fabricate inexpensively and with high throughput. Thus, we have realized a novel, inexpensive, and readily accessible device for real-time characterization of nanoparticle dispersions, which eliminates the time-consuming sample preparation and image analysis required by traditional characterization techniques. It is compatible and hence can be integrated with most of the existing μ-TAS.

As a conclusion, the main scientific results and contributions are summarized.

- For a first time, a diffraction grating, operating under total internal reflection, is applied for investigation and analysis of nanoscaled dispersions.

- All experiments are realized by an autonomous integrated microfluidic detection system, which is based on well-established micro-electro-mechanical systems (MEMS)-fabrication methods.

Acknowledgment. The work is mainly supported by AvH Foundation and partly through the Grants (I.C.) VEGA No. 2/4008/04 and APVT No. APVT-20-017304.

References

(1) van de Hulst, H. *Light scattering by small particles*; Wiley: New York, 1957.
(2) Champion, J.; Meeten, G.; Senior, M. *J. Coll. Interface Sci.* **1979**, *72*, 471−482.
(3) Garcia-Valenzuela, A.; Barrera, R.; Sanchez-Perez, C.; Reyes-Coronado, A.; Mendez, E. *Opt. Express* **2005**, *13*, 6723.
(4) Champion, J.; Meeten, G.; Senior, M. *J. Chem. Soc., Faraday Trans. 2* **1978**, *74*, 1319−1329.
(5) Mohammadi, M. *Adv. Colloid Interface. Sci.* **1995**, *62*, 17.
(6) Meeten, G. *Opt. Commun.* **1997**, *134*, 233.
(7) Sarov, Y.; Nikolaeva, M.; Sendova-Vassileva, M.; Malinovska, D.; Pivin, J. *Vacuum* **2002**, *69*, 321.
(8) Sarov, Y.; Capek, I.; Janíčková, S.; Kostič, I.; Konečníková, A.; Matay, L.; Sarova, V. *Vacuum* **2004**, *76*, 231.
(9) Iadicicco, A.; Campopiano, S.; Cutolo, A.; Giordano, M.; Cusano, A. *IEEE Photon. Technol. Lett.* **2005**, *17*, 1250.
(10) Zourob, M.; Mohr, S.; Fielden, P.; Goddard, N. *Lab Chip* **2005**, *5*, 772.
(11) Anderson, B.; Brodsky, A.; Burgess, L. *Phys. Rev. E* **1996**, *54*, 912.
(12) Brodsky, B.; Burgess, L.; Brodsky, A. *Anal. Chem*. **1996**, *68*, 1081.
(13) Anderson, B.; Brodsky, A.; Burgess, L. *Langmuir* **1997**, *13*, 4273.
(14) Smith, S.; Brodsky, A.; Vahey, P.; Burgess, L. *Anal. Chem.* **2000**, *72*, 4249.
(15) Sainov, S. *Sens. Actuators, A* **1994**, *45*, 1.
(16) Sainov, S.; Tontchev, D. *Opt. Laser Eng.* **1989**, *10*, 17.
(17) Sarov, Y.; Sainov, S. *J. Opt. A: Pure Appl. Opt.* **2002**, *4*, 382.
(18) Ovchinnikov, V.; Udoev, U. *Opt. Spectrosc.* **1978**, *45*, 202.
(19) Sarov, Y.; Ivanova, K.; Ivanov, T.; Volland, B. E.; Rangelow, I. W. *Microelectron. Eng.* **2006**, *83*, 1294.
(20) Sarov, Y.; Ivanov, T.; Ivanova, K.; Sarova, V.; Capek, I.; Rangelow, I. W. *Appl. Phys. A* **2006**, *84*, 191.

(21) Sarov, Y.; Capek, I.; Andok, R.; Sarova, V.; Ivanova, K.; Ivanov, T.; Kostic, I.; Rangelow, I. W. In *Proceedings of the 12th International Workshop on Applied Physics Condense Matter (APCOM 2006)*; Weis, M., Vajda, J., Eds.; The Publishing House of Slovak Technical University: Bratislava, Slovakia, 2006; p 318.
(22) Sarov, Y.; Kostič, I.; Minov, S.; Mitkov, S.; Minchev, G.; Uher, L. *Proc SPIE-Int. Opt. Soc. Eng.* **2003**, *5226*, 194.
(23) Clarke, D.; Crainger, J. *Polarized light and optical measurement*; Pergamon Press: New York, 1971.

NL073260O